


# ATLAS highlights: Recent results from ATLAS

Petr Balek<sup>1,\*</sup>, on behalf of the ATLAS Collaboration

<sup>1</sup>AGH University of Krakow, al. Adama Mickiewicza 30, 30-059 Kraków, Poland

**Abstract.** The ATLAS experiment at the Large Hadron Collider encompasses a wide-ranging physics programme that includes various collision systems and centre-of-mass energies. These proceedings provide an overview of the recent ATLAS measurements regarding heavy ion collisions, heavy flavour production, and collective behaviour. The data utilized in the presented results were recorded during LHC Run 2 (2015–2018). The measurements can help to understand various physics phenomena from hard scatterings to soft processes, and from large systems to small systems.

## 1 Introduction

The heavy-ion programme of the ATLAS experiment at the Large Hadron Collider [1] is rich and encompasses collision systems of different sizes. In the large systems, Pb+Pb and Xe+Xe collisions, it explores the phenomenon of jet quenching in quark-gluon plasma (QGP) and its dependency on the sub-structure, colour charge, or quark flavour of jets, as well as collective effects in QGP such as the azimuthal anisotropy or transverse momentum ( $p_T$ ) fluctuations. In the small collision systems,  $pp$  and  $p$ +Pb, the programme focuses on the origin of collectivity, the formation of quarkonia, and the mechanism behind the jet modification. Furthermore,  $\gamma+\gamma$  and  $\gamma$ +Pb collisions are studied using intense photon fluxes accompanying Pb+Pb collisions.

## 2 ATLAS detector

The ATLAS experiment [1] at the LHC is a multipurpose particle detector with a forward–backward symmetric cylindrical geometry and a near  $4\pi$  coverage in solid angle. It consists of an inner tracking detector surrounded by a thin superconducting solenoid providing a 2 T axial magnetic field, electromagnetic and hadronic calorimeters, and a muon spectrometer. A two-level trigger system is used to select events.

Heavy-ion events are categorized into centrality intervals using the Glauber model parameterization of the  $\Sigma E_T$  distribution in the forward calorimeter [2]. Each centrality interval represents a range in  $\Sigma E_T$ , starting at 0% for the most central collisions.

---

\*e-mail: petr.balek@cern.ch

## 3 Recent ATLAS analyses

### 3.1 Production of $t\bar{t}$ pairs in $p+\text{Pb}$ collisions

The measurement of top-quark production in  $p+\text{Pb}$  collision may provide new constraints for nuclear parton distribution functions (nPDFs) in Bjorken- $x$  about 0.005–0.05 and in  $Q^2$  about  $m_t^2 \approx 3 \times 10^4 \text{ GeV}^2$ , where  $m_t$  denotes top quark mass. Information about gluon nPDF may also be extracted. Anti-shadowing and EMC effects are expected to be responsible for an enhancement of  $\sim 10\%$  in the  $t\bar{t}$  production in  $p+\text{Pb}$  with respect to  $pp$  collisions.

The analysis of  $t\bar{t}$  pairs production [3] uses  $165 \text{ nb}^{-1}$  of  $p+\text{Pb}$  data at  $\sqrt{s_{\text{NN}}} = 8.16 \text{ TeV}$  and focuses on two decay channels. In the single-lepton channel, it selects events with the decay mode  $t\bar{t} \rightarrow W^-\bar{b} + W^+b \rightarrow \ell^-\bar{\nu}_\ell + \bar{b} + q\bar{q} + b$  and analogical process for  $W^+$ . The events are required to have one electron or muon and at least four jets; out of these jets, at least one jet has to be  $b$ -tagged [4]. In the di-lepton channel, both  $W$ -bosons have to decay leptonically:  $t\bar{t} \rightarrow W^-\bar{b} + W^+b \rightarrow \ell^-\bar{\nu}_\ell + \bar{b} + \ell^+\nu_\ell + b$ . Thus, the events are required to have two oppositely charged leptons and at least two jets while at least one jet has to be  $b$ -tagged. Events with the same lepton-flavour pairs with the invariant mass  $80 < m_{\ell\ell} < 100 \text{ GeV}$  are rejected to exclude  $Z$  candidates. The background comes from  $W$  and  $Z$  bosons produced in association with jets, from single  $t$  production, and from di-boson production.

The signal events are simulated using next-to-leading-order Monte Carlo (MC) event generator POWHEG BOX v2 [5], while PYTHIA generator [6] is used for the modelling of parton shower and hadronisation. The background  $Z$ +jets,  $W$ +jets, and di-bosons+jets events are simulated with SHERPA [7]; the background  $t$  and  $tW$  events are simulated with POWHEG BOX v2. The signal and background samples are produced in  $pp$  and  $pn$  configurations, and then embedded to the real  $p+\text{Pb}$  events. This way, their underlying-event contribution is the same as in the data.

The largest systematic uncertainties arise from the jets reconstruction, signal modelling, background modelling, luminosity measurement, and other smaller sources, in this order.

The signal and background events are studied as a function of  $H_T^{\ell,j}$ , a scalar sum of  $p_T$  of all leptons and jets within the event. The signal strength is then extracted using profile-likelihood fit. The post-fit  $H_T^{\ell,j}$  distributions are shown in Figure 1 for both single- and di-lepton channels. The value of measured inclusive cross-section of  $t\bar{t}$  pair production in  $p+\text{Pb}$  collisions is  $\sigma_{t\bar{t}} = 58.1 \pm 2.0 \text{ (stat.)}^{+4.8}_{-4.4} \text{ (syst.)}$ .

Figure 2 (left) shows the measured cross-section in comparison with several MC models, CMS  $p+\text{Pb}$  measurement [8], and ATLAS+CMS  $pp$  measurement [9]. Figure 2 (right) shows the nuclear modification factor, defined as the ratio of  $p+\text{Pb}$  and  $pp$  cross sections, measured at the same  $\sqrt{s_{\text{NN}}}$  energy, scaled by the number of nucleons in the Pb nucleus. For this comparison,  $pp$  cross section is extrapolated from  $\sqrt{s} = 8 \text{ TeV}$  to  $\sqrt{s} = 8.16 \text{ TeV}$ . The nuclear modification factor is  $R_{\text{pA}} = 1.090 \pm 0.039 \text{ (stat.)}^{+0.094}_{-0.087} \text{ (syst.)}$ .

### 3.2 Azimuthal correlations of muon pairs in $\text{Pb}+\text{Pb}$ collisions

Since heavy-flavour quarks cannot be produced thermally in QGP, they are mostly produced in the hard scattering at the early stages of the collisions and thus experience the whole QGP evolution. The quarks may suffer energy loss due to their interactions with the QGP. Additionally, anisotropy of the heavy-flavour quarks, or their decay products, is usually present and can be described by Fourier coefficients  $v_n$ .

The analysis of muon pairs originating in the decays of charm and bottom quarks [10] uses  $\text{Pb}+\text{Pb}$  and  $pp$  data at  $\sqrt{s_{\text{NN}}} = 5.02 \text{ TeV}$  with integrated luminosities of  $1.94 \text{ nb}^{-1}$  and  $0.26 \text{ fb}^{-1}$ , respectively. Muons considered for this analysis are required to have  $p_T > 4 \text{ GeV}$

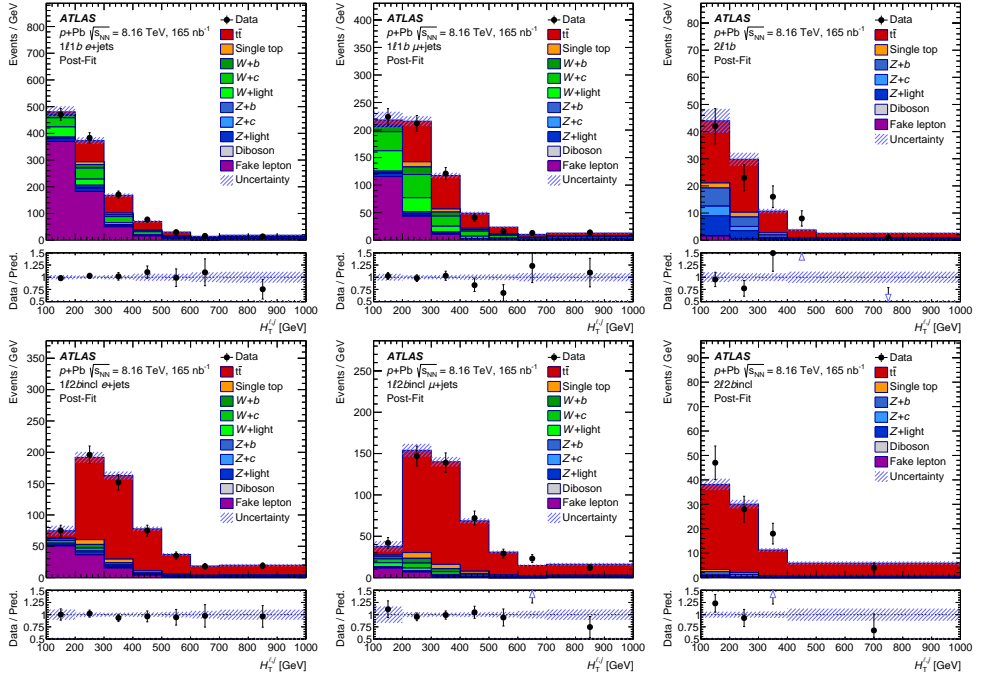


Figure 1: Post-fit distributions of  $H_T^{\ell,j}$  [3]. The distributions are shown for 1  $b$ -tagged jet (top row) and 2  $b$ -tagged jets (bottom row); for single-electron channel (left column), single-muon channel (middle column), and two-lepton channels (right column). Data are shown with black markers, signal with red histogram, and background with histograms of other colours.

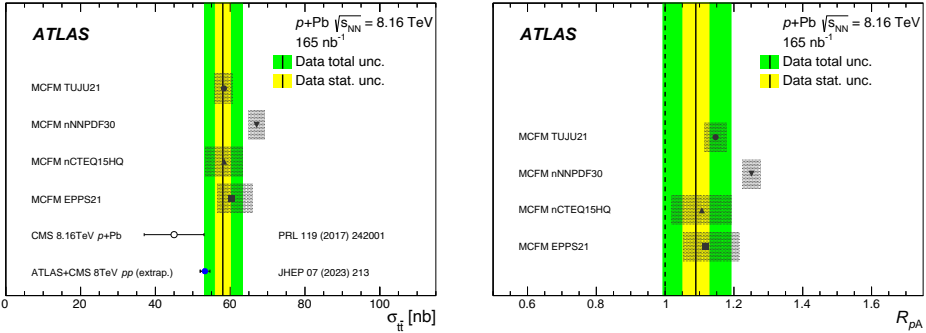
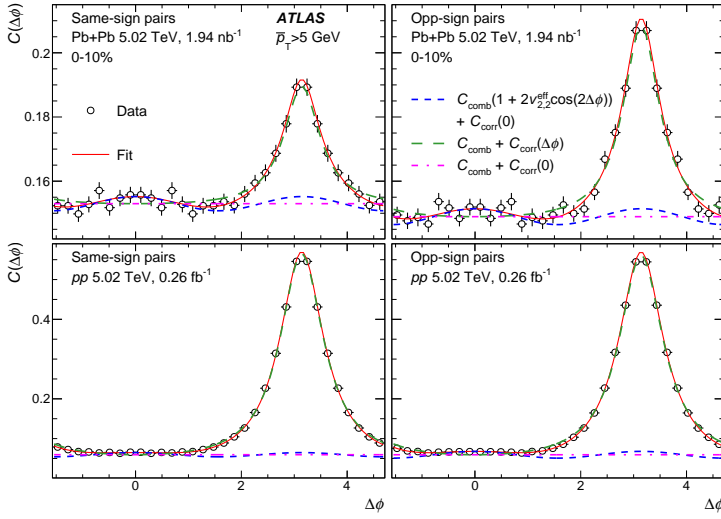
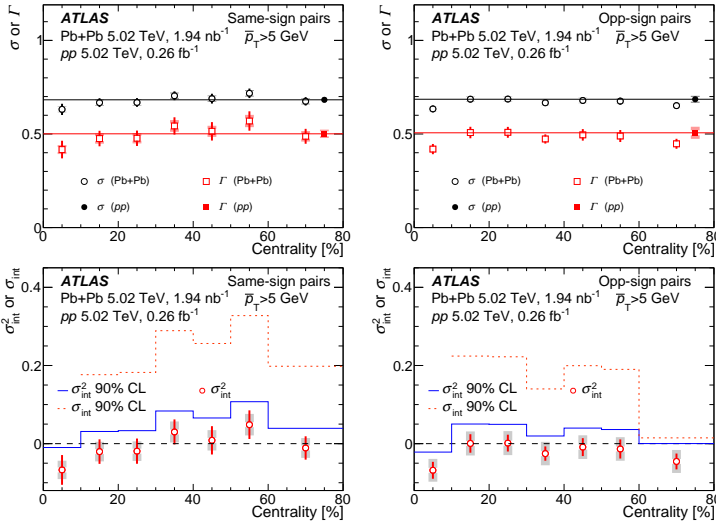


Figure 2: **Left:** Measured cross section of  $t\bar{t}$  production in  $p+Pb$  collisions [3] compared to MC predictions as well as previous CMS and ATLAS results [8, 9]. **Right:** Nuclear modification factor  $R_{pA}$  compared to several MC predictions [3].

and  $|\eta| < 2.4$ . To suppress pairs with low trigger efficiency, the average  $p_T$  of the pair has to be above 5 GeV. To suppress contributions from quarkonia decays and from the production within jets, the muons distance in pseudorapidity has to be more than 0.8; this eliminates decay products of light vector mesons and  $J/\psi$ . Opposite-sign pairs with invariant mass  $9.2 < m_{\mu\mu} < 10.4$  GeV or  $70 < m_{\mu\mu} < 110$  GeV are excluded to eliminate contributions from  $\Upsilon$



**Figure 3.** Distributions of azimuthal angle separation,  $\Delta\phi$ , for same-sign (left column) and opposite-sign (right column) muons pairs in central Pb+Pb (top row) and  $pp$  (bottom row) collisions [10]. The red solid line shows the full template fit of the data; the dashed magenta, green, and blue lines show the contribution of pedestal, pedestal with Breit-Wigner distribution, and pedestal with elliptic flow modulation, respectively.



**Figure 4. Top:** Centrality dependence of  $\Gamma$  and  $\sigma$  widths for same-sign (left) and opposite-sign (right) muon pairs [10]. **Bottom:** Centrality dependence of additional angular deflection introduced by the QGP for same-sign (left) and opposite-sign (right) muon pairs and their 90% confidence levels (CL) [10].

and  $Z$ , respectively. In Pb+Pb, di-muons originating in  $\gamma+\gamma$  scattering are also rejected [11]. To correct for trigger and reconstruction inefficiencies, as well as for the exclusion of the opposite-sign pairs mentioned above, a weight is assigned to each pair [11].

The systematic uncertainties arise from the muon quality selection, trigger and reconstruction efficiency corrections, correction for the  $m_{\mu\mu}$  exclusion, background parametrization, and the method used to extract the observables.

The muon pairs are studied in terms of their azimuthal angle separation,  $\Delta\phi$ , shown in Figure 3. All the correlation functions,  $C(\Delta\phi)$ , show a clear enhancement at  $\Delta\phi = \pi$  on top of a pedestal. The pedestal is significantly higher for Pb+Pb collisions. The correlation functions are fitted with a sum of the flat pedestal, elliptic flow modulation, and Breit-Wigner distribution. The former two terms are from a combinatorial contribution while the third one

is from a correlated contribution:

$$C_{fit}(\Delta\phi) = C_{comb} [1 + 2v_2 \cos(2\Delta\phi)] + C_{corr,max} \Gamma^2 / [(\Delta\phi - \pi)^2 + \Gamma^2]$$

Figure 4 (top) shows centrality dependence of  $\Gamma$  and  $\sigma$ , a standard deviation of  $C(\Delta\phi)$  in  $0 < \Delta\phi < 2\pi$ . There is almost no variation of either with centrality; they both exhibit similar behaviour for same-sign and opposite-sign pairs. Figure 4 (bottom) shows centrality dependence of additional angular deflection due to the presence of QGP,  $\sigma_{int}^2 = \sigma_{PbPb}^2 - \sigma_{pp}^2$ . The 90% confidence levels for  $\sigma_{int}^2$  and  $\sigma_{int}$  are evaluated using combined statistical and systematic uncertainties, providing a model-independent constraint on the stochastic deflection in the QGP.

### 3.3 Speed of sound and $p_T$ fluctuations in Xe+Xe and Pb+Pb collisions

The hydrodynamic expansion of the QGP is not only responsible for the anisotropic flow but also induces a significant boost to the transverse momentum of the particles. This translates to the variation in the mean  $p_T$  in each event,  $[p_T]$ , which is a sensitive probe of QGP properties, such as the equation of state and the associated speed-of-sound,  $c_s$ , in the plasma.

The study of momentum fluctuations [12] uses Pb+Pb collisions at  $\sqrt{s_{NN}} = 5.02$  TeV and Xe+Xe collisions at  $\sqrt{s_{NN}} = 5.44$  TeV with luminosities of  $470 \mu\text{b}^{-1}$  and  $3 \mu\text{b}^{-1}$ , respectively. Events with pileup, i.e. multiple inelastic collisions, are rejected. Tracks considered in this analysis have  $p_T > 5$  GeV and  $|\eta| < 2.5$ . The track reconstruction efficiency and the fake rate are estimated using events generated by HUNG [13]. A weight,  $w_i$ , is applied to each particle in an event to compensate for the fake rate and the reconstruction inefficiency. The charged particle multiplicity corrected for detector effects is denoted by  $N_{ch} = \sum_i w_i$ .

Systematic uncertainties arise from the track selection, detector material modelling, residual pileup, centrality definition, and MC closure check.

The  $[p_T]$ , dimensionless normalized variance,  $k_2$ , and skewness,  $k_3$ , are calculated as:

$$[p_T] = \frac{\sum_i w_i p_{T,i}}{\sum_i w_i}, \quad k_2 = \frac{\sum_{i \neq j} w_i w_j \delta p_{T,i} \delta p_{T,j}}{\langle [p_T] \rangle^2 \sum_{i \neq j} w_i w_j}, \quad k_3 = \frac{\sum_{i \neq j \neq k} w_i w_j w_k \delta p_{T,i} \delta p_{T,j} \delta p_{T,k}}{\langle [p_T] \rangle^3 \sum_{i \neq j \neq k} w_i w_j w_k},$$

where summing is done over all tracks in the event and (for  $k_2$  and  $k_3$ ) over non-repeating unique sets of indices;  $\delta p_{T,i} \equiv p_{T,i} - \langle [p_T] \rangle$ ; and angle brackets,  $\langle \dots \rangle$ , denote the average over all events in the ensemble. In the scenario of independent particle production from participating nucleons,  $N_{ch}$  is roughly proportional to  $N_{part}$ . Consequently, it is expected that  $k_2 \approx N_{ch}^{-1}$  and  $k_3 \approx N_{ch}^{-2}$ .

Figure 5 (left) presents  $k_2$  and  $k_3$  scaled by  $N_{ch}$  and  $N_{ch}^2$ , respectively. Both values rise up to  $N_{ch} \approx 1500$  for both systems. Then, only for Pb+Pb collisions, they show only a little dependence on  $N_{ch}$  in the range  $2000 \lesssim N_{ch} \lesssim 4000$ . In even more central collisions,  $N_{ch} k_2$  displays a sharp decrease, while  $N_{ch}^2 k_3$  shows an abrupt increase followed by a sharp decrease; this is true for both Pb+Pb and Xe+Xe. Such behaviour can be described by models incorporating both geometrical and intrinsic fluctuations of the particle production sources [14].

The increase of  $[p_T]$  is related to the speed of sound in the QGP:

$$c_s^2(T_{\text{eff}}) \propto \frac{d \ln(\langle [p_T] \rangle)}{d \ln(N_{ch})} \approx \frac{\Delta p_T / \langle [p_T] \rangle}{\Delta N_{ch} / \langle N_{ch} \rangle}$$

where  $T_{\text{eff}}$  is the effective temperature of QGP. The fraction can be understood as the slope in Figure 5 (right). An agreement with Music model [14] is achieved for  $c_s^2 \approx 0.23$  and  $T_{\text{eff}} = 222$  MeV. Nevertheless, these values depend on several choices of the analysis, such as the selected  $p_T$  range of the particles.

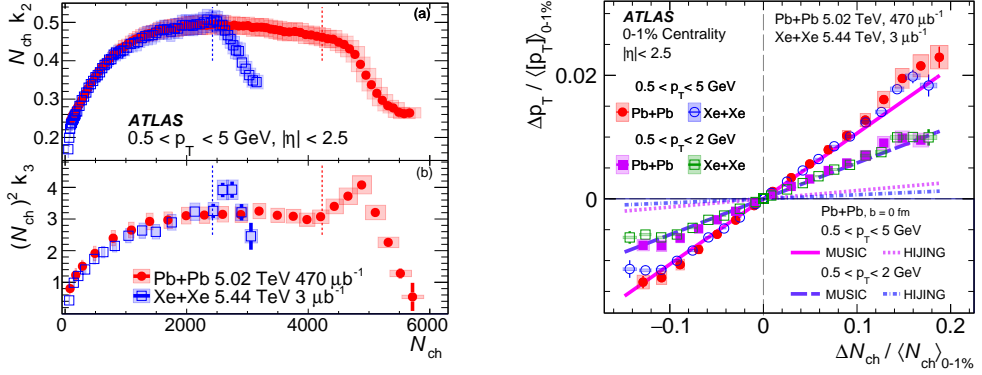


Figure 5: **Left:** Dimensionless normalized variance  $k_2$  scaled by  $N_{ch}$  (top) and dimensionless normalized skewness  $k_3$  scaled by  $N_{ch}^2$  (bottom) as a function of  $N_{ch}$  in Pb+Pb and Xe+Xe collisions [12]. The vertical dashed lines indicate the  $N_{ch}$  values corresponding to 5% centrality in both systems. **Right:** Correlation between  $\Delta p_T / \langle [p_T] \rangle$  and  $\Delta N_{ch} / \langle N_{ch} \rangle$  in the 0-1% most central Pb+Pb and Xe+Xe collisions [12]. Data are compared to calculations of the MUSIC and HIJING models [13, 14]. Both are presented for two  $p_T$  ranges of the particles.

## 4 Summary & Acknowledgements

In the 21st International Conference on Strangeness in Quark Matter (SQM 2024), the ATLAS experiment presented several new results, utilizing data recorded during Run 2 of the LHC. This included the production of  $t\bar{t}$  pairs in  $p$ +Pb collisions, azimuthal correlations of muons in Pb+Pb collisions, and the study  $p_T$  fluctuations with its implications to the speed of sound in QGP in Xe+Xe and Pb+Pb collisions.

This research project is supported by the programme “Excellence Initiative – Research University” for the AGH University in Krakow, application #9041.

## References

- [1] ATLAS Collaboration, JINST **3**, S08003 (2008).
- [2] ATLAS Collaboration, JHEP **01**, 051 (2020), arXiv:1904.04808.
- [3] ATLAS Collaboration (2024), arXiv:2405.05078.
- [4] ATLAS Collaboration, Eur. Phys. J. C **79**, 970 (2019), arXiv:1907.05120.
- [5] S. Alioli, P. Nason, C. Oleari, E. Re, JHEP **06**, 043 (2010), arXiv:1002.2581.
- [6] T. Sjöstrand et al., Comput. Phys. Commun. **191**, 159 (2015), arXiv:1410.3012.
- [7] E. Bothmann et al., SciPost Phys. **7**, 034 (2019), arXiv:1905.09127.
- [8] CMS Collaboration, Phys. Rev. Lett. **119**, 242001 (2017), arXiv:1709.07411.
- [9] ATLAS and CMS Collaborations, JHEP **07**, 213 (2023), arXiv:2205.13830.
- [10] ATLAS Collaboration, Phys. Rev. Lett. **132**, 202301 (2024), arXiv:2308.16652.
- [11] ATLAS Collaboration, Phys. Rev. C **107**, 054907 (2023), arXiv:2206.12594.
- [12] ATLAS Collaboration (2024), arXiv:2407.06413.
- [13] X.N. Wang, M. Gyulassy, Phys. Rev. D **44**, 3501 (1991).
- [14] B. Schenke et al., Phys. Rev. C **82**, 014903 (2010), arXiv:1004.1408.